Journal of Electrochemistry

Volume 26
Issue 2 *Special Issue : High Temperature Electrochemistry*

2020-04-28

NiO@rGO Supported Palladium and Silver Nanoparticles as Electrocatalysts for Oxygen Reduction Reaction

Shuo YAO

Tai-zhong HUANG
1. Shandong Provincial Key Laboratory of Fluorine Chemistry Material, School of Chemistry and Chemical Engineering, University of Jinan, Jinan 250022, China;, chm_huangtz@ujn.edu.cn

Rizwan HAIDER

Heng-yi FANG

Jie-mei YU

Zhan-kun JIANG

Dong LIANG

See next page for additional authors

Recommended Citation

Shuo YAO, Tai-zhong HUANG, Rizwan HAIDER, Heng-yi FANG, Jie-mei YU, Zhan-kun JIANG, Dong LIANG, Yue SUN, Xian-xia YUAN. NiO@rGO Supported Palladium and Silver Nanoparticles as Electrocatalysts for Oxygen Reduction Reaction[J]. *Journal of Electrochemistry*, 2020 , 26(2): 270-280.
DOI: 10.13208/j.electrochem.190125
Available at: https://jelectrochem.xmu.edu.cn/journal/vol26/iss2/15

NiO@rGO Supported Palladium and Silver Nanoparticles as Electrocatalysts for Oxygen Reduction Reaction

Authors

Shuo YAO, Tai-zhong HUANG, Rizwan HAIDER, Heng-yi FANG, Jie-mei YU, Zhan-kun JIANG, Dong LIANG, Yue SUN, and Xian-xia YUAN

Corresponding Author(s)

Tai-zhong HUANG(chm_huangtz@ujn.edu.cn);
Xian-xia YUAN(yuanxx@sjtu.edu.cn)

DOI: 10.13208/j.electrochem.190125 **Article ID**:1006-3471(2020)02-0270-11
Cite this: *J. Electrochem.* **2020**, *26*(2): 270-280 **Http**://electrochem.xmu.edu.cn

NiO@rGO Supported Palladium and Silver Nanoparticles as Electrocatalysts for Oxygen Reduction Reaction

YAO Shuo[1,2], HUANG Tai-zhong[1*], HAIDER Rizwan[2], FANG Heng-yi[1],
YU Jie-mei[1], JIANG Zhan-kun[1], LIANG Dong[1], SUN Yue[1], YUAN Xian-xia[2*]
(1. *Shandong Provincial Key Laboratory of Fluorine Chemistry Material, School of Chemistry and Chemical Engineering, University of Jinan, Jinan* 250022, *China*; 2. *Department of Chemical Engineering, Shanghai Jiao Tong University, Shanghai* 200240, *China*)

Abstract: For pervasive applications of fuel cells, highly efficient and economical materials are required to replace Pt-based catalysts for oxygen reduction reaction (ORR). In this study, the NiO@rGO, Pd-NiO@rGO and Ag-NiO@rGO nanoparticles were synthesized, and their catalytic performances toward ORR were investigated. The results revealed that all the three materials were capable of catalyzing ORR, but both the Pd-NiO@rGO and Ag-NiO@rGO showed the better performances compared with the NiO@rGO in terms of the reaction pathway being 4-electron process, the increases of the onset potential and the intermediate yielding rate, as well as the extended stability. Moreover, the effect of Pd modification was superior to that of Ag.

Key words: oxygen reduction reaction; catalyst; nickel oxide; reduced graphene oxide; surface modification
CLC Number: O646 **Document Code:** A

The performance and efficiency of fuel cells are majorly affected by the sluggish cathodic oxygen reduction reaction (ORR)[1-3]. At present, platinum (Pt) -based catalysts are considered as an efficient catalyst for ORR[4-6]. However, the scarce resource and expensive cost hinder large-scale applications, and impede the development and commercialization of fuel cells. Moreover, the Pt-based catalysts are susceptible to generate a mixed potential especially in direct methanol fuel cells due to the crossover of methanol from anode to cathode[7-8]. Thus, it is necessary to develop alternative materials with high stability, low cost and superior activity.

In the past decade, non-precious metal based catalysts for ORR, including transition metal oxides (TMOs) and chalcogenides[9-11], metal-carbon nitrides[12-14], metal-organic frameworks (MOFs)[15], and so on, have been widely investigated[16-17]. Among these materials, TMOs are in spotlight due to their facile synthesis, low cost and high chemical stability[18-20]. For example, Kumar et al.[21] reported well-disseminated Co_3O_4 nanoparticles supported on reduced graphene oxide (rGO), which exhibited striking performance compared to the commercial Pt/C (10wt%) catalyst. Nickel oxide (NiO) is a p-type antiferromagnetic semiconductor, which has many potential applications in lithium ion batteries and fuel cell materials, owing to its wide band gap (3.5 eV)[22-24]. However, the applications of pure NiO particles are inhibited by slow electron transport and low catalytic sites due to easy aggregation and staking. With the merits of extremely high specific surface area, good conductivity and exceptional thermal/electrical conductivity[25-28], reduced graphene oxide (rGO) is usually used as a support to enhance the dispersity and activity of catalysts[29]. Li et al.[30] fabricated a flower-like NiO@rGO hybrid, in which NiO was tightly wrapped in rGO matrix. The synergistic effect of NiO and rGO made the NiO@rGO hybrid showed better electrochemical performance compared with pristine NiO. Sun et al.[28]

Received: 2019-01-25, Revised: 2019-04-08 * Corresponding author, Tel: (86-21)54742827, E-mail: yuanxx@sjtu.edu.cn; Tel: (86)13589038189, E-mail: chm_huangtz@ujn.edu.cn

reported various rGO supported TMOs (FeO_x, MnO_x, CoO_x and CuO_x) nanocomposites as a catalyst for ORR. The above mentioned nanocomposites showed the enhanced electro-catalytic performance over bare TMOs in an alkaline electrolyte. In order to further improve the catalytic activity of TMOs, some researchers have investigated loading a small amount of precious metals on TMOs@rGO, which displayed much better performances. CeO_2@rGO supported Pt nanoparticles exhibited excellent catalytic activity, while Ag-CeO_2/rGO ternary nanocomposite also exhibited good stability and surpassing catalytic activity[31-32].

Pd and Ag are adjacent to Pt in the periodic table, and they have similar chemical and physical properties to Pt. Among the catalysts studied before, Pd-based and Ag-based catalysts are promising Pt-alternative catalysts for ORR due to their comparable performance to Pt in an alkaline medium[6]. So far there has been no comprehensive study reporting the catalytic activity of NiO@rGO supported Pd and/or Ag for ORR. Herein, NiO@rGO was prepared by pyrolysis of $Ni(OH)_2$/graphene oxide (GO) at 400 ℃ in a N_2 atmosphere, and followed by loading Pd and Ag nanoparticles via a simple $NaBH_4$ reduction method. Microstructure and electrochemical catalytic performance of the as-prepared materials were compared and are discussed.

1 Experimental

1.1 Material Syntheses

All chemical reagents were utilized as purchased without further purification. The GO suspension was prepared from graphite power following improved Hummers' method[33]. Sulfuric acid (H_2SO_4, 98%, 115 mL) was mixed slowly with graphite powder (3.00 g), and followed by cooling in an ice-water bath. $KMnO_4$ (15.00 g) was then added into the mixture with vigorous stirring for 12 h. The obtained blackish green oily liquid was poured into 200 mL ultrapure water along with continuous stirring. Thenceforth, 15 mL H_2O_2 (30%) was added into the obtained mixture with 2 h of extended stirring to bring in golden yellow suspension, and followed by alternative washing with 1 mol·L^{-1} H_2SO_4 and ultrapure water. The obtained suspension was then dispersed into ultrapure water to get 6 mg·mL^{-1} GO suspension.

0.50 g of $NiSO_4 \cdot 6H_2O$ and 0.25 g of NaOH were dissolved separately in ultrapure water. The NaOH solution was added dropwise into the $NiSO_4$ solution with regular stirring to precipitate green $Ni(OH)_2$, then followed by repeated washing with ultrapure water. In the meantime, 5 mL of GO suspension was mixed with 100 mL of ultrapure water and sonicated for 30 min to get homogeneous suspension. The washed $Ni(OH)_2$ was then added into the suspension and sonicated for another 1 h. Afterwards, the mixture was collected, washed and then dried at 60 ℃ for 10 h to obtain $Ni(OH)_2$/GO. Subsequently, the $Ni(OH)_2$/GO was heated in a N_2 atmosphere at 400 ℃ for 4 h to obtain NiO@rGO powder.

The Pd-NiO@rGO catalyst was prepared following a typical methodology as described below: 0.10 g of the prepared NiO@rGO powder was added into 50 mL ultrapure water, and followed by the addition of 10 mL $PdCl_2$ solution (2.34 mg·mL^{-1}) along with robust stirring. The Pd(II) ions in the solution were reduced by adding, dropwise, 50 mL of 0.1 mol·L^{-1} $NaBH_4$ aqueous solution counting 1 h of vigorous stirring followed by another 1 h sonication. The obtained precipitate was washed and dried at 60 ℃. Ag-NiO@rGO catalyst was prepared by the same route, using 2.24 mg·mL^{-1} $AgNO_3$ solution instead of the $PdCl_2$ solution.

1.2 Material Characterizations

Phase components of the catalysts were characterized by X-ray diffraction (XRD) tests using Bruker D8-advance diffractometer with a Cu K_α irradiation source (λ = 1.5418 Å) within 2θ range from 10° to 80°. Morphologies of the as-prepared catalysts were determined using Hitachi S-4800 scanning electron microscope (SEM). Transmission electron microscope (TEM) images were filmed using Hitachi Tecnai 20 U-TWIN instrument. X-ray photoelectron spectroscope (XPS) measurements were carried out using Perkin Elmer PHI5300 spectrometer equipped with monochromatized Mg K_α radiation.

1.3 Electrochemical Measurements

Electrochemical tests were conducted by using

CHI 750D potentiostat/galvanostat with three-electrode system. Herein, the glassy carbon electrode with smeared catalyst was used as the working electrode, while saturated calomel electrode (SCE) and platinum wire were adopted as the reference and counter electrode, respectively. The working electrode was prepared as follows: a mixture of 450 μL ultrapure water, 50 μL Nafion solution (5% in aliphatic alcohols) and 5 mg catalyst powder was ultrasonicated for 40 min to obtain a homogeneous suspension ink. Then, 5 μL of the obtained ink was dropped onto the glassy carbon electrode (3 mm in diameter), which had been freshly polished with 0.05 μm alumina powder and fully dried.

Electrochemical measurements were conducted in 0.1 mol·L^{-1} KOH electrolyte. Before actual data recording, high purity N_2 was bubbled through the electrolyte for 30 min to remove the dissolved oxygen from air and the working electrode was cycled at a scanning rate of 5 mV·s^{-1} between 0.2 and -0.8 V (vs. SCE, E(RHE) = E(SCE)+0.998, 0.1 mol·L^{-1} KOH) at room temperature until the reproducible results were obtained. The electrolyte was then saturated with oxygen followed by recording of cyclic voltammetry (CV) curves and Tafel plots at room temperature with a potential scanning rate of 5 mV·s^{-1}. The long-term running stability was evaluated at half wave potential for 6000 s.

The rotating disc electrode (RDE) tests were performed with the scanning rate of 5 mV·s^{-1} at various rotating rates, using RRDE-3A rotating system combined with CHI 750D electrochemical workstation.

2 Results and Discussion

Fig. 1(A) displays the XRD patterns of the as-prepared materials. Five peaks at 2θ = 37.1°, 43.1°, 62.6°, 75.0° and 79.0° were evident in all diffractograms, which are corresponding to the (111), (200), (220), (311) and (222) planes of cubic NiO (JCPDS No. 65-2901). In the Pd-NiO@rGO pattern, the peaks at 40.1°, 46.7° and 68.2° could be assigned, respectively, to (111), (200) and (220) facets of metallic Pd (JCPDS No. 65-6174). Furthermore, the peaks at

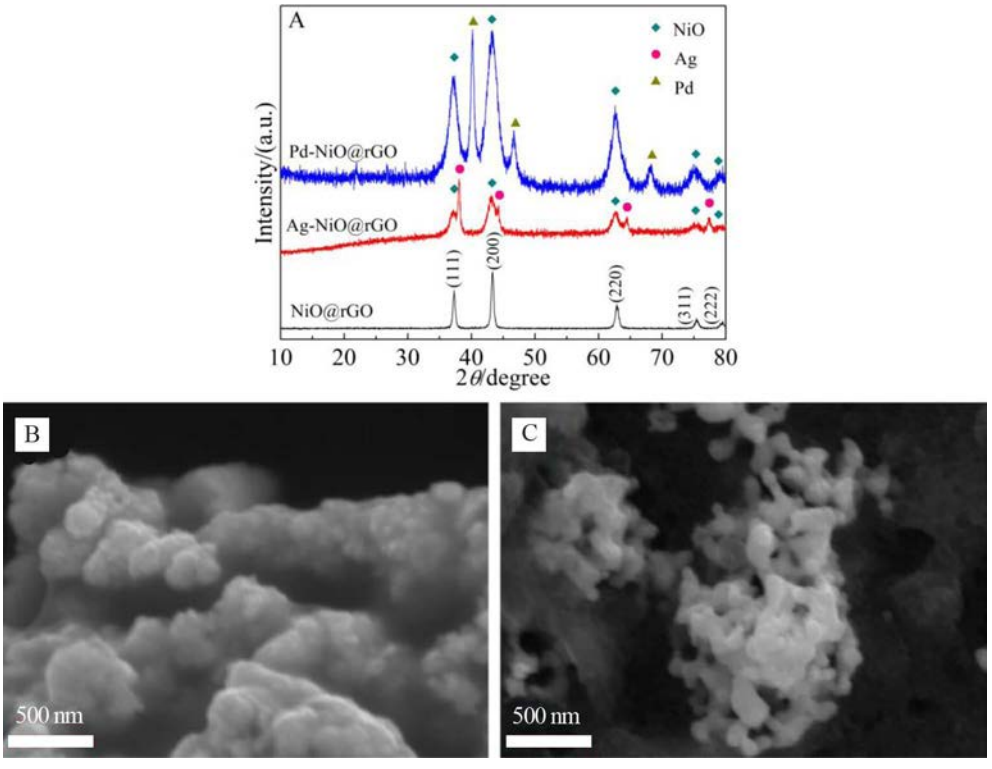

Fig. 1 (A) XRD patterns of NiO@rGO, Pd-NiO@rGO and Ag-NiO@rGO. SEM images of Pd-NiO@rGO (B) and Ag-NiO@rGO (C)

38.2°, 44.3°, 64.4° and 77.4° in Ag-NiO@rGO were accordingly attributed to (111), (200), (220) and (311) facets of metallic Ag (JCPDS No. 65-2871). These results indicate that the metallic Pd and Ag had been successfully loaded onto the surface of NiO@rGO. Moreover, no observation of miscellaneous peaks implies high purity of the as-prepared catalysts. Fig. 1(B) and Fig. 1(C) show the SEM images of the Pd-NiO@rGO and Ag-NiO@rGO catalysts, respectively. The development of physical cross-linking sites in the rGO hydrogel frame-work could be observed due to overlapping or coalescing of flexible rGO[34]. In Fig. 1(B), the sphere-like Pd-NiO particles with different sizes were observed on the rGO surface. Fig. 1(C) displays the dendrite-like porous Ag-NiO particles.

Fig. 2(A) and Fig. 2(C) show the TEM images of Pd-NiO@rGO and Ag-NiO@rGO, respectively. It could be seen that the sphere-like Pd-NiO and dendritic-like Ag-NiO particles were distributed on rGO. Fig. 2(B) shows the HRTEM image of Pd-NiO@rGO. The crystal lattice distances of 0.224 and 0.209 nm could be indexed to (111) facet of Pd and (200) facet of NiO, respectively. Similarly, the crystal distances of 0.237 and 0.210 nm in the TEM image of Ag-NiO@rGO in Fig. 2(D) should be attributed to (111) facet of Ag and (200) facet of NiO, respectively. The results were consistent with the XRD patterns as discussed above. In addition, the rGO lattice was also clearly observed in the HRTEM images of both catalysts. The results proved the successful synthesis of Pd-NiO@rGO and Ag-NiO@rGO catalysts.

To investigate the binding state of the compositional elements of the catalysts, the high resolution XPS spectra of Ni, Pd and Ag are provided in Fig. 3. It could be seen from Fig. 3(A) that the peaks centered at 856.8 and 875.1 eV for Pd-NiO@rGO were corresponding to Ni $2p_{3/2}$ and Ni $2p_{1/2}$, respectively, while the couple peaks at 862.1 and 881.1 eV were shake-up satellite peaks. Likewise, for the Ag-NiO@rGO in Fig. 3(B), the Ni $2p_{3/2}$ and Ni $2p_{1/2}$ peaks were centered at 856.1 and 874.4 eV, respectively, with satellite

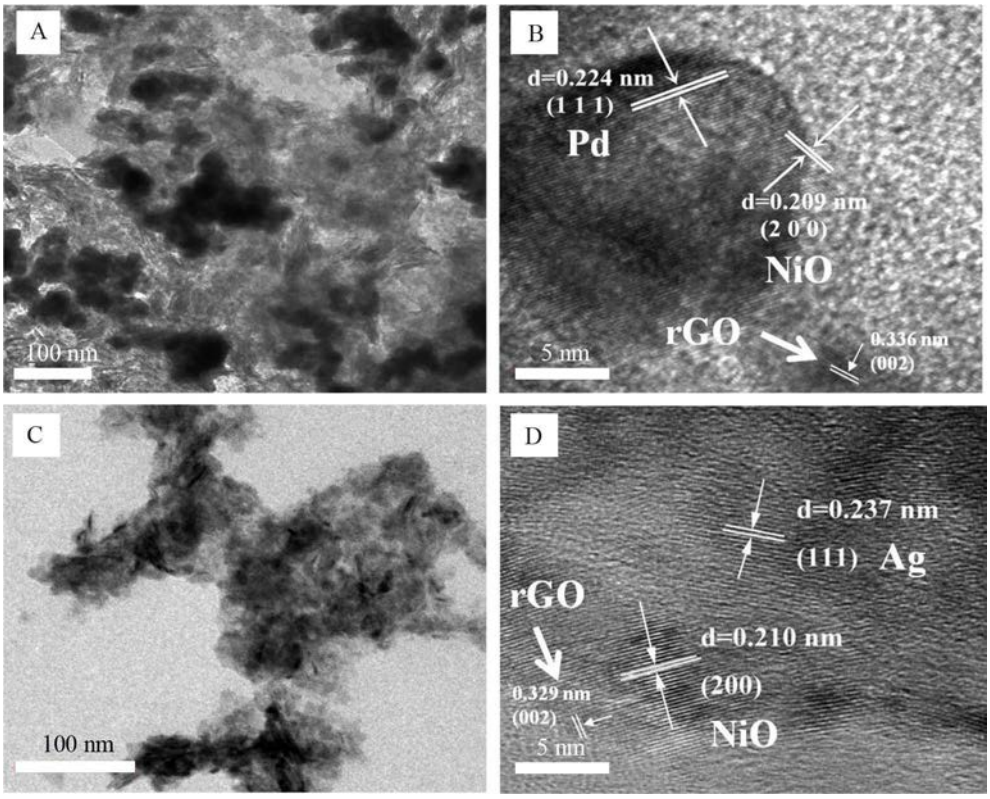

Fig. 2 TEM and HRTEM images of Pd-NiO@rGO (A, B) and Ag-NiO@rGO (C, D)

peaks at 861.9 and 880.7 eV. Both catalysts showed the same spin-orbit difference (18.3 eV) between $2p_{3/2}$ and $2p_{1/2}$. The results indicated the successful synthesis of NiO in the as-prepared catalysts[35-36]. Fig. 3(C) illustrates the deconvoluted peaks of Pd 3d at 335.3 and 340.5 eV, which could be assigned to $3d_{5/2}$ and $3d_{3/2}$, respectively[37-38]. The calculated spin-orbital separation of 5.2 eV illustrates that metallic Pd had been successfully loaded on the surface of catalysts[39]. In the 3d spectra of Ag in Fig. 3(D), two peaks centered at 368.4 and 374.4 eV could be assigned to $3d_{5/2}$ and $3d_{3/2}$, respectively, and the calculated spin-orbital separation value of 6 eV illustrated the zero valence of Ag[40].

Electrochemical performance of the as-prepared catalysts toward ORR was comparatively investigated. Fig. 4(A) to Fig. 4(C) display the CV curves of Pd-NiO@rGO, Ag-NiO@rGO and NiO@rGO in N_2- and O_2-saturated 0.1 mol·L^{-1} KOH electrolytes with the scanning rate of 5 mV·s^{-1}. It is clearly shown that in the N_2-saturated electrolyte, there were no peaks observed for all materials, while clear cathodic peaks were seen in the O_2-saturated electrolyte. This result means that all the catalysts were chemically/electrochemically stable in the electrolyte, while they were catalytically efficient toward ORR. For a comparative study of ORR activity, the CV curves in O_2-saturated electrolyte are overlapped in Fig. 4(D). It is obviously shown that the Pd-NiO@rGO and Ag-NiO@rGO catalysts had higher onset potentials and peak current densities for ORR compared with the NiO@rGO, suggesting that ORR is easier to take place on the NiO@rGO supported Pd and Ag catalysts. On the other hand, the Pd-NiO@rGO (0.574 mA·mg^{-1}) catalyst exhibited higher mass activity toward ORR than the Ag-NiO@rGO (0.422 mA·mg^{-1}) and NiO@rGO

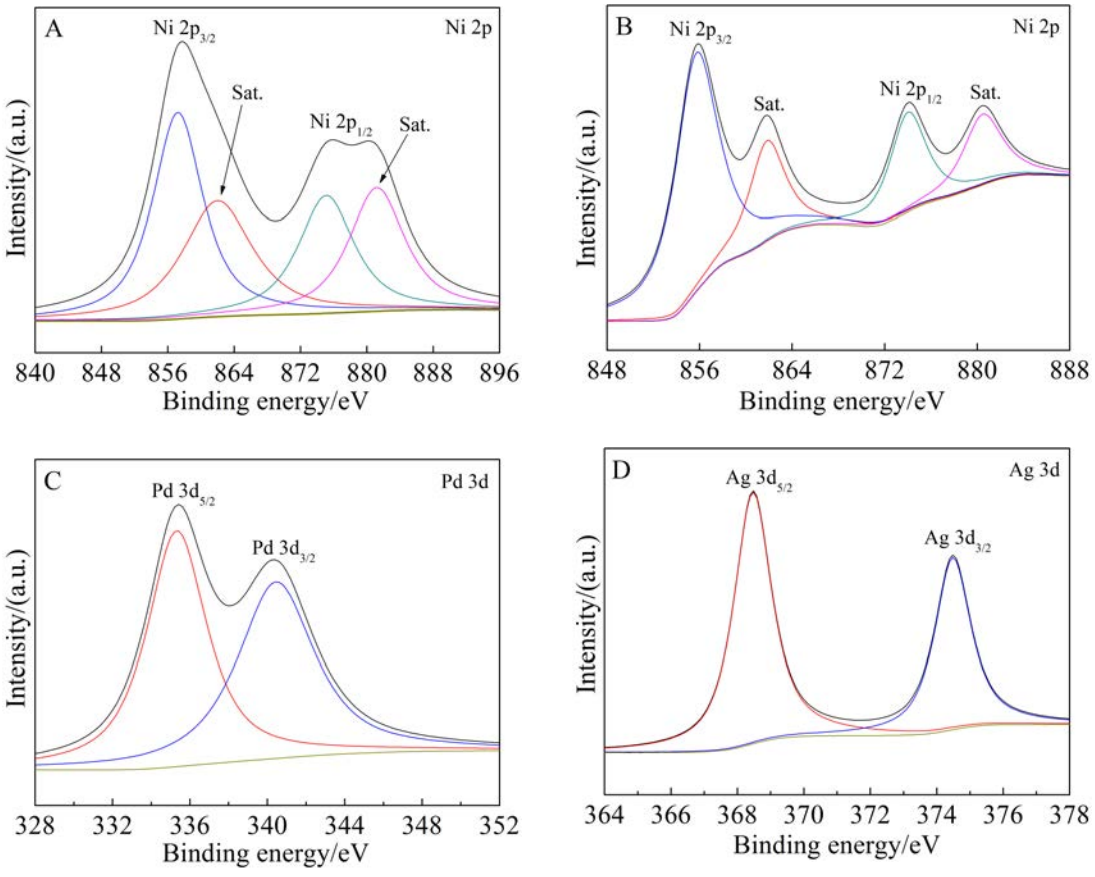

Fig. 3 High resolution XPS spectra of Ni 2p in Pd-NiO@rGO (A) and Ag-NiO@rGO (B), Pd 3d in Pd-NiO@rGO (C) and Ag 3d in Ag-NiO@rGO (D)

(0.376 mA·mg^{-1}). Furthermore, the peak potential of Pd-NiO@rGO (0.75 V vs. RHE) was more positive than that of Ag-NiO@rGO (0.48 V vs. RHE), which also indicates the higher energy catalytic activity of Pd-NiO@rGO.

To further investigate the catalytic performance of the catalysts, the Tafel tests were conducted and the results are shown in Fig. 4(E). Based on the Tafel tests, the Tafel slope (b) could be obtained and the values are displayed in Table 1. On the other hand, the exchange current density (i_0) and electron transfer coefficient (α) are generally calculated using Tafel equation (1) [38]:

$$\eta = -\frac{RT}{\alpha nF}\lg i_0 + \frac{RT}{\alpha nF}\lg i \quad (1)$$

where η and i are the measured overpotential and current density, respectively. R is the gas constant (8.314 J·mol^{-1}·K^{-1}), F is the Faraday constant (96485 C·mol^{-1}), T is the temperature in K, n is the electron transfer number. The calculated values of α and i_0 are

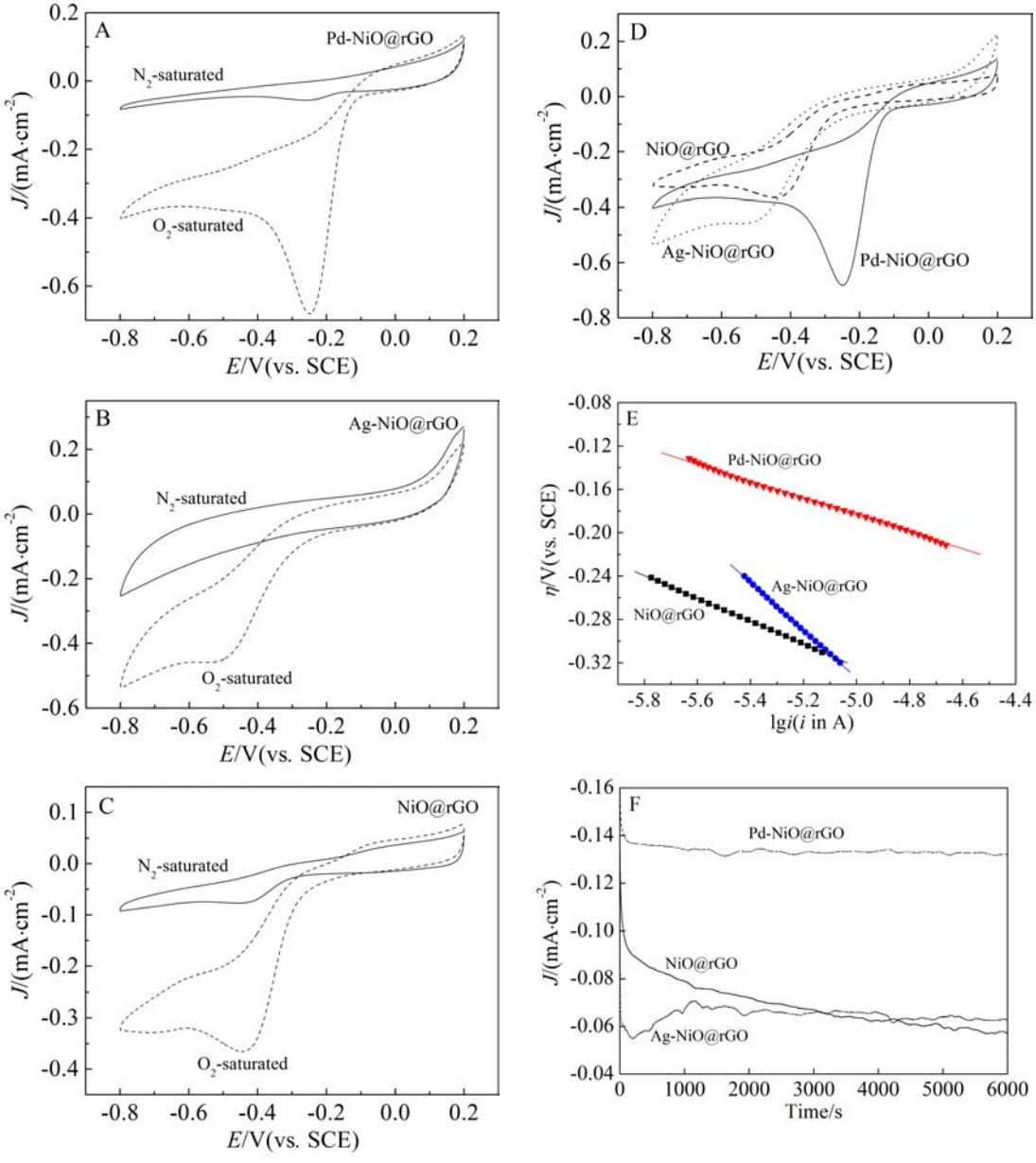

Fig. 4 CV curves of Pd-NiO@rGO (A), Ag-NiO@rGO (B) and NiO@rGO (C) in the N_2- and O_2-saturated 0.1 mol·L^{-1} KOH electrolytes with the scanning rate of 5 mV·s^{-1}; (D) comparison of CV curves, (E) Tafel plots and (F) chronoamperometric curves of Pd-NiO@rGO, Ag-NiO@rGO and NiO@rGO.

also listed in Tab. 1. The largest α and the maximum i_0 of Pd-NiO@rGO in Tab. 1 represent swift electron transfer kinetics and fast electrode kinetics as compared with those of Ag-NiO@rGO and NiO@rGO.

Tab. 1 Tafel slope b, electron transfer coefficient (α), exchange current density (i_0), and transfer electron number (n) of Pd-NiO@rGO, Ag-NiO@rGO and NiO@rGO catalyzed ORR

Catalyst	b/(V·dec^{-1})	α	i_0/(A·cm^{-2})	n
Pd-NiO@rGO	0.078	0.0625	8.9×10^{-7}	3.89
Ag-NiO@rGO	0.220	0.0612	7.1×10^{-7}	3.71
NiO@rGO	0.105	0.0298	1.5×10^{-7}	2.36

Long-time running stability is one of the most important characteristics for ORR electrocatalysts. The chronoamperometric current-time curves of Pd-NiO@rGO, Ag-NiO@rGO and NiO@rGO are displayed in Fig. 4(F). It was clearly observed that the current densities of Pd-NiO@rGO and Ag-NiO@rGO catalyzed ORR, after 6000 s, were larger than that of NiO@rGO (0.056 mA·cm^{-2}). The Pd-NiO@rGO and Ag-NiO@rGO catalysts were more stable than the bare NiO@rGO. The current density of Ag-NiO@rGO (0.062 mA·cm^{-2}) was only slightly increased as compared with that of the NiO@rGO. The Pd-NiO@rGO (0.133 mA·cm^{-2}) catalyzed ORR showed more than double higher current intensity than the pristine NiO@rGO. Therefore, it could be concluded that the modifications of both Pd and Ag on NiO@rGO can escalate the stability of NiO@rGO for ORR. It was also clearly shown that the effect of Pd became more outstanding than that of the commercial Pt/C catalyst. RDE tests of the catalysts were conducted in 0.1 mol·L^{-1} KOH solution with various rotating rates to investigate the catalytic performances of Pd-NiO@rGO, Ag-NiO@rGO and NiO@rGO toward ORR, and the background corrected polarization curves are presented in Fig. 5(A) to Fig. 5(C). It was noticeable that, to each catalyst, the current density was increased with the increase of rotating rate, which should be attributed to the enhanced oxygen diffusion on the electrode surface[41]. The limiting current density at each rotating rate changing from low to high was in the order of NiO@rGO, Ag-NiO@rGO and Pd-NiO@rGO. The electron transferred number (n) for ORR can be calculated according to RDE tests and the corresponding Koutecky-Levich (K-L) plots are drawn based on the following equation[42]:

$$J^{-1} = J_K^{-1} + J_L^{-1} = J_K^{-1} + B\omega^{-1/2} \quad (2)$$

where J is the measured current density, J_K is the kinetic current density and J_L is the diffusion-limiting current density, ω is the electrode rotation rate and B is the slope of K-L plot which can be expressed by the following equation[43]:

$$B = 0.62nF(D_0)^{2/3}v^{-1/6}C_0 \quad (3)$$

In Eq. (3), C_0 (1.2×10^{-6} mol·cm^{-3}) is the bulk concentration of oxygen in the electrolyte, D_0 (1.9×10^{-5} cm^2·s^{-1}) is the diffusion coefficient of oxygen in 0.1 mol·L^{-1} KOH and v (0.01 cm^2·s^{-1}) is the kinetic viscosity of the electrolyte. Therefore, when J^{-1} is plotted against $\omega^{-1/2}$, the slope of the obtained line could be used to determine the value of n. The obtained K-L plots are displayed in Fig. 5(D) to Fig. 5(F) using the current densities at 0.45, 0.50, 0.55 and 0.60 V. The calculated values of n for the Pd-NiO@rGO (3.89) and Ag-NiO@rGO (3.71) were evidently larger than that for bare NiO@rGO (2.36) as listed in Tab. 1. For an oxygen reduction reaction, the 4-electron process is more favorable than the 2-electron process by virtue of the faster reaction kinetics and low percentage of yielded intermediate, i.e., hydrogen peroxide (H_2O_2%)[44]. The 4-electron and 2-electron ORR pathways are given as following:

The 4-electron process:

$$O_2 + 2H_2O + 4e \rightarrow 4OH^- \quad (4)$$

The 2-electron process:

$$O_2 + 2H_2O + 2e \rightarrow 2OH^- + H_2O_2 \quad (5)$$

$$H_2O_2 + 2e \rightarrow 2OH^- \quad (6)$$

Based on the RDE tests, it could be deduced that, with the catalyses of Pd-NiO@rGO and Ag-NiO@rGO, the ORR majorly happened through 4-electron style, while the catalysis of NiO@rGO through 2-electorn pathway[45-46]. The synergistic effect of Ag and Pd on NiO@rGO boosted the kinetics and reduced the intermediate yield of ORR[47].

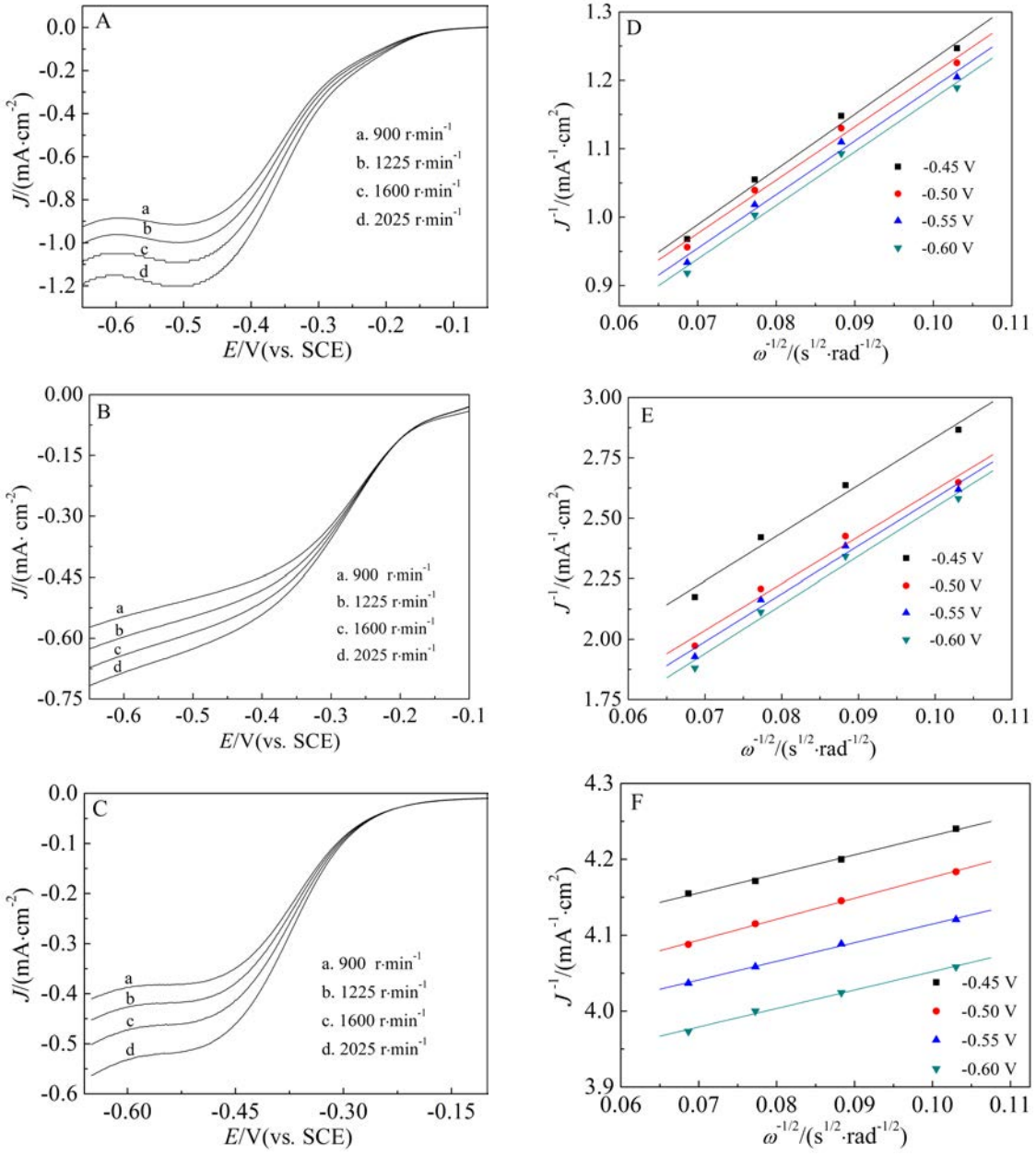

Fig. 5 RDE polarization curves and the corresponding K-L plots of Pd-NiO@rGO(A, D), Ag-NiO@rGO (B, E) and NiO@rGO (C, F) with different electrode rotating speeds in O_2-saturated 0.1 mol·L^{-1} KOH electrolyte with the scanning rate of 5 mV·s^{-1}

3 Conclusions

The NiO@rGO was prepared by a facile route. The metallic Pd and Ag were then successfully loaded on to obtain the catalysts of Pd-NiO@rGO and Ag-NiO@rGO. Comparative studies in their catalytic performance for ORR showed that both Pd and Ag could boost up the ORR kinetics from 2-electron to 4-electron process. The catalytic activity and long time running stability were improved by the synergistic effect between metals and the NiO@rGO support. This research demonstrates a novel methodology of developing high performance catalysts using transition metal oxides.

Acknowledgements

This project was financially supported by National Natural Science Foundation of China (No.

21476138), Shandong Natural Science Foundation (No. ZR2018MB036 and No. ZR2017QB009), Science Development Project of Shandong Province (No. 2017GGX40115 and No. 2016GGX102038), Project of Shandong Province Higher Educational Science and Technology Program (No. J17KA094, No. J13LD08), Scientific Research Fund of University of Jinan (No. XBS1644).

References:

[1] Liu Q, Zhang J Y. Graphene supported Co-g-C_3N_4 as a novel metal-macrocyclic electrocatalyst for the oxygen reduction reaction in fuel cells[J]. Langmuir, 2013, 29(11): 3821-3828.

[2] Zhao Y, Ding Y, Qiao B, et al. Interfacial proton enrichment enhances proton-coupled electrocatalytic reactions [J]. Journal of Materials Chemistry A, 2018, 6(36): 17771-17777.

[3] Xue Q, Bai J, Han C C, et al. Au nanowires@Pd-polyethylenimine nanohybrids as highly active and methanol-tolerant electrocatalysts toward oxygen reduction reaction in alkaline media[J]. ACS Catalysis, 2018, 8(12): 11287-11295.

[4] Jayasayee K, Van Veen JAR, Manivasagam T G, et al. Oxygen reduction reaction (ORR) activity and durability of carbon supported PtM (Co, Ni, Cu) alloys: Influence of particle size and non-noble metals[J]. Applied Catalysis B: Environmental, 2012, 111: 515-526.

[5] Jennings P C, Pollet B G, Johnston R L. Theoretical studies of Pt-Ti nanoparticles for potential use as PEMFC electrocatalysts[J]. Physical Chemistry Chemical Physics, 2012, 14(9): 3134-3139.

[6] Xu G R, Han C C, Zhu Y Y, et al. PdCo alloy nanonetworks-polyallylamine inorganic-organic nanohybrids toward the oxygen reduction reaction[J]. Advanced Materials Interfaces, 2018, 5(4): 1701322.

[7] Dong Y Y, Deng Y J, Zeng J H, et al. A high-performance composite ORR catalyst based on the synergy between binary transition metal nitride and nitrogen-doped reduced graphene oxide[J]. Journal of Materials Chemistry A, 2017, 5(12): 5829-5837.

[8] Xue Q, Xu G R, Mao R D, et al. Polyethyleneimine modified AuPd@PdAu alloy nanocrystals as advanced electrocatalysts towards the oxygen reduction reaction[J]. Journal of Energy Chemistry, 2017, 26(6): 1153-1159.

[9] Roche I, Chaînet E, Chatenet M, et al. Carbon-supported manganese oxide nanoparticles as electrocatalysts for the oxygen reduction reaction (ORR) in alkaline medium: Physical characterizations and ORR mechanism[J]. The Journal of Physical Chemistry C, 2007, 111(3): 1434-1443.

[10] Zhou J, Xiao H, Zhou B W, et al. Hierarchical MoS_2-rGO nanosheets with high MoS_2 loading with enhanced electro-catalytic performance[J]. Applied Surface Science, 2015, 358: 152-158.

[11] Wu X Y, Gao X P, Xu L P, et al. Mn_2O_3 doping induced the improvement of catalytic performance for oxygen reduction of MnO[J]. International Journal of Hydrogen Energy, 2016, 41(36): 16087-16093.

[12] Xiao M L, Zhu J B, Ma L, et al. Microporous framework induced synthesis of single-atom dispersed Fe-N-C acidic ORR catalyst and its *in situ* reduced Fe-N_4 active site identification revealed by X-ray absorption spectroscopy [J]. ACS Catalysis, 2018, 8(4): 2824-2832.

[13] Cai P W, Peng X X, Huang J H, et al. Covalent organic frameworks derived hollow structured N-doped noble carbon for asymmetric-electrolyte Zn-air battery[J]. Science China Chemistry, 2019, 62(3): 385-392.

[14] Lin Y, Chai G L, Wen Z H. Zn-MOF-74 derived N-doped mesoporous carbon as pH-universal electrocatalyst for oxygen reduction reaction[J]. Advanced Functional Materials, 2017, 27(14): 1606190.

[15] Xia W, Qu C, Liang Z B, et al. High-performance energy storage and conversion materials derived from a single metal-organic framework/graphene aerogel composite[J]. Nano Letters, 2017, 17(5): 2788-2795.

[16] Song P(宋平), Ruan M B(阮明波), Liu J(刘京), et al. Recent research for non-Pt-based oxygen reduction reaction electrocatalysts in fuel cell[J]. Journal of Electrochemistry(电化学), 2015, 21(2): 130-137.

[17] Cai P W, Li Y, Wang G X, et al. Alkaline-acid Zn-H_2O fuel cell for simultaneous generation of hydrogen and electricity[J]. Angewandte Chemie International Edition, 2018, 57(15): 3910-3915.

[18] Osgood H, Devaguptapu S V, Xu H, et al. Transition metal (Fe, Co, Ni, and Mn) oxides for oxygen reduction and evolution bifunctional catalysts in alkaline media[J]. Nano Today, 2016, 11(5): 601-625.

[19] Kalantar-Zadeh K, Ou J Z, Daeneke T, et al. Two dimensional and layered transition metal oxides[J]. Applied Materials Today, 2016, 5: 73-89.

[20] Wang D C, Huang N B, Sun Y, et al. GO clad Co_3O_4 (Co_3O_4@GO) as ORR catalyst of anion exchange membrane fuel cell[J]. International Journal of Hydrogen Energy, 2017, 42(31): 20216-20223.

[21] Kumar K, Canaff C, Rousseau J, et al. Effect of the oxide-carbon heterointerface on the activity of Co_3O_4/NRGO nanocomposites towards ORR and OER[J]. Journal of Physical Chemistry C, 2016, 120(15): 7949-7958.

[22] Amin R S, Hameed R M A, El-Khatib K M, et al. Pt-NiO/C anode electrocatalysts for direct methanol fuel cells[J]. Electrochimica Acta, 2012, 59: 499-508.

[23] Tong S F, Zheng M B, Lu Y, et al. Mesoporous NiO with a single-crystalline structure utilized as a noble metal-free catalyst for non-aqueous Li-O_2 batteries[J]. Journal of Materials Chemistry A, 2015, 3(31): 16177-16182.

[24] Xu X B, Liu Z H, Zuo Z X, et al. Hole selective NiO contact for efficient perovskite solar cells with carbon electrode[J]. Nano Letters, 2015, 15(4): 2402-2408.

[25] Zhao J, Yu H, Liu Z S, et al. Supercritical deposition route of preparing Pt/graphene composites and their catalytic performance toward methanol electrooxidation [J]. Journal of Physical Chemistry C, 2014, 118(2): 1182-1190.

[26] Geng D, Ding N, Hor T S A, et al. Potential of metal-free "graphene alloy" as electrocatalysts for oxygen reduction reaction[J]. Journal of Materials Chemistry A, 2015, 3(5): 1795-1810.

[27] Higgins D, Zamani P, Yu A, et al. The application of graphene and its composites in oxygen reduction electrocatalysis: a perspective and review of recent progress[J]. Energy & Environmental Science, 2016, 9(2): 357-390.

[28] Sun M, Liu H J, Liu Y, et al. Graphene-based transition metal oxide nanocomposites for the oxygen reduction reaction[J]. Nanoscale, 2015, 7(4): 1250-1269.

[29] Xiu L Y(修陆洋), Yu M Z(于梦舟), Yang P J(杨鹏举), et al. Caging porous Co-N-C nanocomposites in 3D graphene as active and aggregation-resistant electrocatalyst for oxygen reduction reaction[J]. Journal of Electrochemistry (电化学), 2018, 24(6): 715-725.

[30] Li X J, Fan L l, Li X F, et al. Enhanced anode performance of flower-like NiO/RGO nanocomposites for lithium-ion batteries[J]. Materials Chemistry and Physics, 2018, 217: 547-552.

[31] Yu S P, Liu Q B, Yang W S, et al. Graphene-CeO_2 hybrid support for Pt nanoparticles as potential electrocatalyst for direct methanol fuel cells[J]. Electrochimica Acta, 2013, 94: 245-251.

[32] Ji Z Y, Shen X P, Yang J L, et al. A novel reduced graphene oxide/Ag/CeO_2 ternary nanocomposite: Green synthesis and catalytic properties[J]. Applied Catalysis B: Environmental, 2014, 144: 454-461.

[33] Hummers W S, Offeman R E. Preparation of graphitic oxide[J]. Journal of the American Chemical Society, 1958, 80(6): 1339.

[34] Chang K, Chen W X. L-cysteine-assisted synthesis of layered MoS_2/graphene composites with excellent electrochemical performances for lithium ion batteries[J]. ACS Nano, 2011, 5(6): 4720-4728.

[35] Wen M, Sun B L, Zhou B, et al. Controllable assembly of Ag/C/Ni magnetic nanocables and its low activation energy dehydrogenation catalysis[J]. Journal of Materials Chemistry, 2012, 22(24): 11988-11993.

[36] Wanger C D, Riggs W M, Davis L E, et al. Handbook of X-ray photoelectron spectroscopy[M]. Minnesota: Perkin-Elmer Corp., Physical Electronics Division, 1979.

[37] Zhang J, Liu H L, Wang B, et al. Preparation of Pd/GO/Ti electrode and its electrochemical degradation for 2,4-dichlorophenol[J]. Materials & Design, 2015, 86(Supplement C): 664-669.

[38] Kahri H, Sevim M. Enhanced catalytic activity of monodispersed AgPd alloy nanoparticles assembled on mesoporous graphitic carbon nitride for the hydrolytic dehydrogenation of ammonia borane under sunlight[J]. Nano Research, 2017, 10(5): 1627-1640.

[39] Zhao X H, Liu X. A novel magnetic $NiFe_2O_4$@graphene-Pd multifunctional nanocomposite for practical catalytic application[J]. RSC Advances, 2015, 5(97): 79548-79555.

[40] Yang L, Luo W, Cheng G Z. Graphene-supported ag-based core-shell nanoparticles for hydrogen generation in hydrolysis of ammonia borane and methylamine borane[J]. ACS Applied Materials & Interfaces, 2013, 5(16): 8231-8240.

[41] Gong K P, Du F, Xia Z H, et al. Nitrogen-doped carbon nanotube arrays with high electrocatalytic activity for oxygen reduction[J]. Science, 2009, 323(5915): 760-764.

[42] Wei Y C, Liu C W, Wang K W. Improvement of oxygen reduction reaction and methanol tolerance characteristics for PdCo electrocatalysts by Au alloying and CO treatment[J]. Chemical Communications, 2011, 47(43): 11927-11929.

[43] Alexiadis A, Cornell A, Dudukovic M P. Comparison between CFD calculations of the flow in a rotating disk cell and the Cochran/Levich equations[J]. Journal of Electroanalytical Chemistry, 2012, 669(1): 55-66.

[44] Gu W L, Hu L Y, Hong W, et al. Noble-metal-free Co_3S_4-S/G porous hybrids as an efficient electrocatalyst for oxygen reduction reaction[J]. Chemical Science, 2016, 7(7): 4167-4173.

[45] Nakabayashi S, Yagi I, Sugiyama N, et al. Reaction pathway of four-electron oxidation of formaldehyde on plat-

inum electrode as observed by *in situ* optical spectroscopy[J]. Surface Science, 1997, 386(1/3): 82-88.

[46] Chang H C, Han C K, Yook S, et al. Hydrogen peroxide synthesis via enhanced two-electron oxygen reduction pathway on carbon-coated Pt surface[J]. Journal of Physical Chemistry C, 2014, 118(51): 30063-30070.

[47] Yin Z, Zhang Y N, Chen K, et al. Monodispersed bimetallic PdAg nanoparticles with twinned structures: Formation and enhancement for the methanol oxidation[J]. Scientific Reports, 2014, 4: 4288.

NiO@rGO 负载钯、银纳米粒子用作氧还原催化剂

姚 硕[1,2], 黄太仲[1*], Rizwan Haider[2], 房恒义[1], 于洁玫[1],
姜占坤[1], 梁 栋[1], 孙 玥[1], 原鲜霞[2*]

(1. 济南大学化学化工学院, 山东省氟化学化工重点实验室, 山东 济南 250022;
2. 上海交通大学化学工程系, 上海 200240)

摘要: 为了促进燃料电池的广泛应用, 必须研发一种高效、经济的氧还原(ORR)催化剂材料替代目前使用的昂贵的 Pt 基催化剂. 本文合成了 NiO@rGO、Pd-NiO@rGO 和 Ag-NiO@rGO 三种催化剂材料, 并对其 ORR 催化性能进行了比较研究. 结果表明, 三种材料均具有催化 ORR 的能力, 但与 NiO@rGO 相比, Pd-NiO@rGO 和 Ag-NiO@rGO 展示了更加优异的性能, 主要表现在其 4 电子转移 ORR 过程、起始电位增加, 中间产物的产率降低和稳定性提高. 其中, Pd-NiO@rGO 作为 ORR 催化剂的性能最好.

关键词: 氧还原; 催化剂; 氧化镍; 还原氧化石墨烯; 表面修饰